



Recognition of nectin-2 by the natural killer cell receptor T cell immunoglobulin and ITIM domain (TIGIT)

Received for publication, March 16, 2017, and in revised form, May 12, 2017. Published, Papers in Press, May 17, 2017, DOI 10.1074/jbc.M117.786483

Felix A. Deuss^{‡§¶}, Benjamin S. Gully^{‡§¶}, Jamie Rossjohn^{‡§¶||1,2}, and Richard Berry^{‡§¶1,3}

From the [‡]Infection and Immunity Program, Biomedicine Discovery Institute and the [§]Department of Biochemistry and Molecular Biology, Monash University, Clayton, Victoria 3800, Australia, the [¶]Australian Research Council Centre of Excellence in Advanced Molecular Imaging, Monash University, Clayton, Victoria 3800, Australia, and the ^{||}Institute of Infection and Immunity, Cardiff University School of Medicine, Cardiff CF14 4XN, United Kingdom

Edited by Luke O'Neill

T cell immunoglobulin and ITIM domain (TIGIT) is an inhibitory receptor expressed on the surface of natural killer (NK) cells. TIGIT recognizes nectin and nectin-like adhesion molecules and thus plays a critical role in the innate immune response to malignant transformation. Although the TIGIT/nectin-like protein-5 (necl-5) interaction is well understood, how TIGIT engages nectin-2, a receptor that is broadly over-expressed in breast and ovarian cancer, remains unknown. Here, we show that TIGIT bound to the immunoglobulin domain of nectin-2 that is most distal from the membrane with an affinity of 6 μM , which was moderately lower than the affinity observed for the TIGIT/necl-5 interaction (3.2 μM). The TIGIT/nectin-2 binding disrupted pre-assembled nectin-2 oligomers, suggesting that receptor-ligand and ligand-ligand associations are mutually exclusive events. Indeed, the crystal structure of TIGIT bound to the first immunoglobulin domain of nectin-2 indicated that the receptor and ligand dock using the same molecular surface and a conserved “lock and key” binding motifs previously observed to mediate nectin/nectin homotypic interactions as well as TIGIT/necl-5 recognition. Using a mutagenesis approach, we dissected the energetic basis for the TIGIT/nectin-2 interaction and revealed that an “aromatic key” of nectin-2 is critical for this interaction, whereas variations in the lock were tolerated. Moreover, we found that the C-C' loop of the ligand dictates the TIGIT binding hierarchy. Altogether, these findings broaden our understanding of nectin/nectin receptor interactions and have implications for better understanding the molecular basis for autoimmune disease and cancer.

Natural killer (NK)⁴ cells are innate lymphocytes that form the front line of defense toward viral infection, malignant trans-

formation, and damaged tissues. NK cell function is governed by the integration of signals received via an array of large receptor families that comprise both inhibitory and activating members. Examples of inhibitory NK cell receptors include members of the KIR (killer cell immunoglobulin-like receptors) and LIR (leukocyte immunoglobulin-like receptors) in humans (1) the Ly49 family in mice (2) and the CD94/NKG2 family in both species (3, 4). These inhibitory receptors typically recognize major histocompatibility complex (MHC)-I molecules that are expressed on the surface of all nucleated cells (5–9). Accordingly, healthy cells that express normal levels of MHC-I are protected from NK cells, whereas virally infected or transformed cells that have reduced MHC-I surface expression are susceptible to NK cell-mediated lysis. This process is termed “missing self” recognition (10).

In addition to the receptors described above, NK cells also encode additional receptor families that do not bind MHC-I molecules. For example, an emerging group of type I cell membrane receptors that includes TIGIT (T cell immunoglobulin and ITIM domain), DNAM-1 (CD226), and CD96 (TACTILE) specifically recognize nectin and nectin-like (necl) adhesion proteins (11–14). Of these, TIGIT is an inhibitory receptor that is also expressed on subsets of regulatory and memory CD4⁺ T cells as well as CD8⁺ T cells. TIGIT possesses a single extracellular immunoglobulin variable (IgV) domain that is responsible for binding nectin-2 (CD112), nectin-3 (CD113), and necl-5 (CD155) (14–16). Ligand binding results in the phosphorylation of Tyr²²⁵ within the immunoglobulin tail tyrosine (ITT)-like motif of TIGIT, which triggers intracellular signaling cascades that serve to limit NK cell activation (17). Notably, several viral proteins have been reported to down-regulate both nectin-2 and necl-5 expression (18–20). Thus, it may be that the primary function of TIGIT is to mediate missing self recognition of virally infected cells. However, nectin-2 and necl-5 are frequently up-regulated in a variety of cancers (21–24). Here TIGIT expression can be counter-productive, because it directly opposes the activity of the activating DNAM-1 receptor, thereby limiting NK cell-mediated cytotoxicity of some tumors *in vitro* (2).

In addition to acting as ligands for nectin receptors, nectin and nectin-like molecules are one of the major constituents of

The authors declare that they have no conflicts of interest with the contents of this article.

The atomic coordinates and structure factors (code 5V52) have been deposited in the Protein Data Bank (<http://www.pdb.org/>).

¹ Both authors are joint senior and corresponding authors.

² Supported by Australian Research Council Laureate Fellowship FL160100049. To whom correspondence may be addressed. Tel.: 61-3-9902-9236; Fax: 99054699; E-mail: Jamie.rossjohn@monash.edu.

³ Supported by Career Development Fellowship Grant APP1109901 from the National Health and Medical Research Council of Australia. To whom correspondence may be addressed. Tel.: 61-3-9902-9239; E-mail: Richard.berry@monash.edu.

⁴ The abbreviations used are: NK, natural killer; KIR, killer cell immunoglobulin-like receptors; TIGIT, T cell immunoglobulin and ITIM domain; SEC-MALS, size exclusion chromatography coupled with multi-angle laser light

scattering; SPR, surface plasmon resonance; EC, ectodomain; PDB, Protein Data Bank; r.m.s., root mean square.

Nectin receptor structure

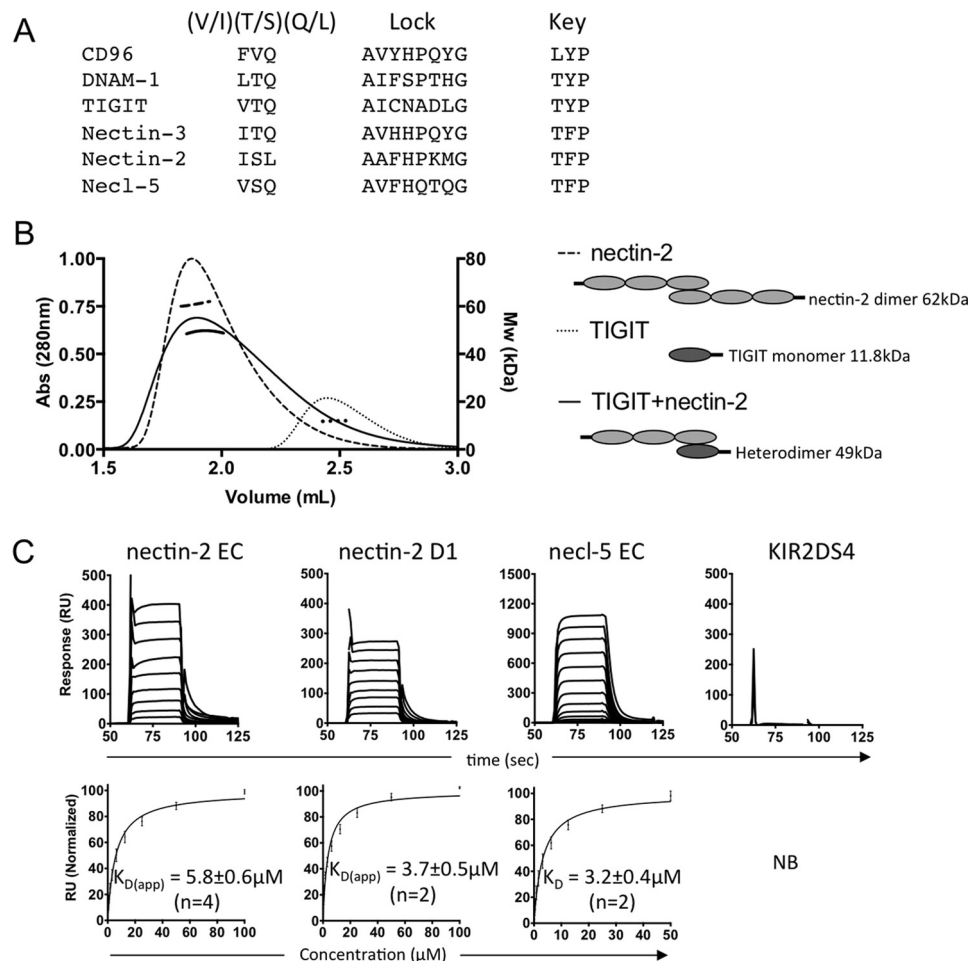


Figure 1. TIGIT/nectin-2 binding. A, sequence alignment of the three conserved motifs found within nectin receptors and their ligands. B, mass measurements and elution profiles of TIGIT, nectin-2, and an equimolar mixture of TIGIT and nectin-2 determined by SEC-MALS. The protein species corresponding to each mass measurement is depicted schematically on the right. C, SPR sensograms (top) and equilibrium binding curves (bottom) are shown for the interaction between soluble nectin-2 EC, nectin-2 D1, necl-5 EC, and KIR2DS4 against immobilized TIGIT. SPR sensograms are representative of a single experiment. Equilibrium binding curves were derived from n independent experiments as denoted. $K_D/K_{D(app)}$ and mean \pm S.E. (depicted as error bars) were calculated from the independent experiments. NB indicates no binding.

adherins junctions and thus play a central role in a number of cellular processes including adhesion, migration, and proliferation (3, 4, 25). Nectin and nectin-like protein function is dependent on their ability to associate into homo- and heterodimers both within the plane of the same membrane (*in cis*) and between opposing cell membranes (*in trans*) to form a tight network of “zippers” between adjacent cells (4). Nectin and necl homo-dimers are formed via interactions between the most membrane distal of their three extracellular Ig domains (D1), which contain signature “lock” and “key” motifs that serve to latch the molecules together (26). Intriguingly, these lock and key motifs are also conserved in the first Ig domain of the nectin receptors and a recent structure of TIGIT bound to necl-5 revealed a binding mode that was similar to that observed for nectin/nectin dimeric interactions (27). However, whether this docking mode is conserved in other receptor-ligand pairings within this axis remains unclear. Here we present a comprehensive structural and biophysical analysis of the TIGIT/nectin-2 interaction that broadens our knowledge of the molecular details underpinning nectin receptor/ligand interactions.

Results

TIGIT binding disrupts nectin-2 oligomerization

To study the interaction between TIGIT and nectin-2, we expressed and purified their corresponding ectodomains from *Escherichia coli* and mammalian expression systems, respectively. Notably, TIGIT and nectin-2 both contain the signature lock and key motifs within their respective D1 domains (Fig. 1A). Thus, to assess whether the recombinant TIGIT and nectin-2 ectodomains associated in solution, we performed size exclusion chromatography coupled with multi-angle laser light scattering (SEC-MALS). Using this approach, nectin-2 eluted at ~ 1.91 ml and had a mass of 62 kDa, approximately twice that expected for a monomer based on amino acid sequence (36.5 kDa) (Fig. 1B). The dimeric status of nectin-2 is in agreement with both structural data and solution-based studies that suggest nectin-2 forms a stable homo-dimer ($K_D \sim 0.4 \mu\text{M}$) in solution (26). By contrast, TIGIT eluted at a volume of ~ 2.47 ml, and had a mass of 11.9 kDa, in good agreement with a monomer based on amino acid sequence (11.7 kDa). The monomeric nature of TIGIT in solution was consistent with previous NMR

and analytical ultracentrifugation data that suggested that the dissociation constant for TIGIT self-association was high ($K_D > 1$ mM) (27). When TIGIT and nectin-2 were pre-mixed at a 1:1 molar ratio, a single peak, with a calculated mass of ~ 49 kDa was evident at 1.93 ml (Fig. 1B). Because this peak was well separated from that observed for the TIGIT monomer, we concluded it represented a TIGIT·nectin-2 complex (predicted mass 48.2 kDa) rather than a mixture of TIGIT monomer and nectin-2 dimer. Accordingly, isolated TIGIT and nectin-2 ectodomains are able to associate in solution and this interaction is concomitant with a dissociation of the nectin-2 homodimer.

TIGIT binds to the first Ig domain of nectin-2 with low micromolar affinity

Although limited cellular staining experiments suggest nectin-2 is a poor ligand for TIGIT (14), our SEC-MALS data suggested that the affinity of TIGIT for nectin-2 was relatively high. To formally assess the strength of the TIGIT/nectin-2 interaction, we performed direct binding studies using surface plasmon resonance (SPR). As a negative control we used the structurally related molecule KIR2DS4, which did not bind to TIGIT (Fig. 1C). In contrast, the entire nectin-2 ectodomain (EC) bound robustly to TIGIT with an apparent affinity ($K_{D(\text{app})}$) of 5.8 ± 0.6 μM (Fig. 1C). Although this affinity was lower than that observed for the binding of TIGIT to nectin-5 ($K_D = 3.2 \pm 0.4$ μM), it was at the higher end of the range typically observed for NK cell receptor/ligand interactions (e.g. KIR3DL1:HLA-B57, $K_D = 17$ μM (8), Ly49C:H2-K^b, $K_D = 80$ μM (28), NKR-P1B:m12, $K_D \sim 6$ μM (29)), suggesting nectin-2 represents a *bona fide* TIGIT ligand. Notably, the second and third Ig domains of nectin-2 appeared to be superfluous to the interaction, because a truncated form of nectin-2 comprising only the first, membrane distal Ig domain (nectin-2-D1) bound to TIGIT with similar affinity ($K_{D(\text{app})} = 3.7 \pm 0.5$ μM) as the entire nectin-2 ectodomain (Fig. 1C). Thus, the first Ig domain of nectin-2 mediates a strong interaction with TIGIT.

Overview of the TIGIT/nectin-2 structure

To understand the molecular basis for the recognition of nectin-2 by TIGIT, we determined the crystal structure of TIGIT bound to nectin-2-D1 to 3.1-Å resolution (Table 1). The structure refined very well, to an $R_{\text{fac}}/R_{\text{free}}$ of 21.4/23.0, respectively, and the electron density at the TIGIT/nectin-2 interface was unambiguous, thereby permitting a detailed understanding of the molecular interactions that underpin the interaction. The crystallographic asymmetric unit comprised two molecules of TIGIT and two molecules of nectin-2 that together formed a symmetrical double-winged structure (Fig. 2A). Within this heterotetrameric arrangement, the two TIGIT molecules form the “body” (see “Discussion”), whereas the nectin-2 molecules lie at the extremities and correspond to the “wings.”

Both TIGIT and nectin-2 D1 adopted β -sandwich-folds (sheet 1, ABED; sheet 2, C'CFG) and possess a strand topology that is classical of the Ig-variable domain superfamily (30). Accordingly, TIGIT and nectin-2 D1 are closely structurally conserved, with a root mean square deviation (r.m.s. deviation) of 1 Å over 80 aligned C α atoms. Although the TIGIT and

Table 1
X-ray crystallographic data collection and refinement statistics

Data collection statistics	
Temperature (K)	100
X-ray source	MX2 Australian Synchrotron
Space group	P4 ₃ 2 ₁ 2
Cell dimensions	68.50, 68.50, 253.91 90, 90, 90
Resolution (Å)	85–3.1 (3.27–3.1)
Total number of observations	81,489 (12,229)
No. unique observations	11,784 (1677)
Multiplicity	6.9 (7.3)
Data completeness	99.8 (100)
$I/\sigma I$	6.3 (1.7)
R_{pim} (%)	9.6 (41)
CC(1/2)	0.986 (0.532)
Refinement statistics	
Non-hydrogen atoms	
Protein	3418
Sugar	25
R_{factor} (%) ^a	21.4
R_{free} (%)	23
R.m.s. deviation from ideality	
Bond lengths (Å)	0.007
Bond angles (°)	0.96
Ramachandran plot	
Favored regions (%)	97.3
Allowed regions (%)	2.4
Disallowed regions (%)	0.3
B factor, all atoms (Å ²)	71

^a $R_{\text{factor}} = \sum_{\text{hkl}} \|F_o - |F_c|/\sum_{\text{hkl}} F_o\|$ for all data excluding the 5% that comprised the R_{free} used for cross-validation.

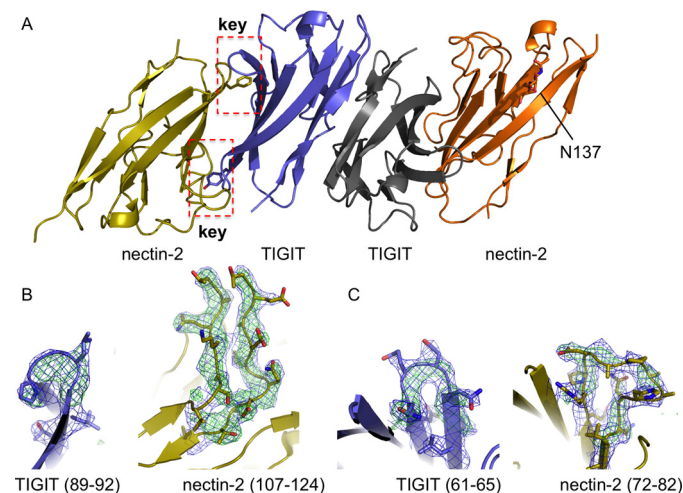


Figure 2. Overview of the TIGIT/nectin-2 structure. A, schematic representation of the TIGIT/nectin-2 heterotetramer. The aromatic key residues (sticks) and the AX₆G locks (denoted by red dashed rectangles) are highlighted for a single TIGIT/nectin-2 interaction. Electron density maps of the TIGIT and nectin-2 DE (B) and C-C' (C) loops. The final refined $2F_o - F_c$ map (blue mesh) and an $F_o - F_c$ omit map (green mesh) are shown contoured at 1σ and 3σ , respectively.

nectin-2 secondary structure elements superpose well, the two molecules differ in the size and conformation of the connecting loops. In particular, the C-C' and D-E loops are markedly extended (by 15 and 5 residues, respectively) in nectin-2, thereby allowing us to confidently verify the identity of each molecule within the electron density map (Fig. 2, B and C). Neither TIGIT nor nectin-2 D1 underwent significant conformational changes upon complex formation (TIGIT r.m.s. deviation 0.42 Å over 96 C α atoms, nectin-2 r.m.s. deviation 0.35 Å over 111 C α atoms) compared with their previously published unliganded forms (PDB codes 3Q0H and 4DFH (31)). A sugar moiety derived from the mammalian expression system is visi-

Nectin receptor structure

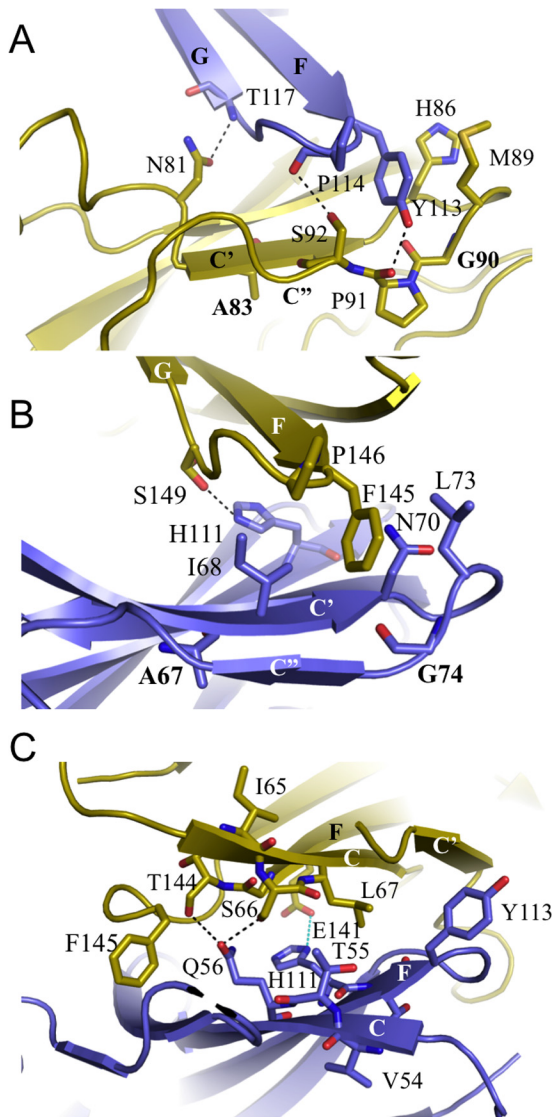


Figure 3. Molecular interactions at the TIGIT/nectin-2 interface. *A*, the key of TIGIT (slate) docking within the lock of nectin-2 (gold) and *B*, the key of nectin-2 docking within the lock of TIGIT. The conserved alanine and glycine residues that cap the pockets are highlighted in **bold**. *C*, interactions involving the (V/I)(S/T)(Q/L) motif. For context, the key residues of nectin-2 (F145) and TIGIT (Y113) are also shown as sticks. *Black dashed lines* indicate hydrogen bonds, *blue dashed lines* denote salt bridges.

ble at the single predicted *N*-linked glycosylation site (Asn¹³⁷) on the F-strand of one of the nectin-2 protomers and does not impact on TIGIT binding (Fig. 2A).

The TIGIT/nectin-2 interface

TIGIT and nectin-2 D1 interacted over a broad region that encompassed the breadth of their corresponding C''C'CFG sheets as well as the interconnecting C''C' and FG loops (Fig. 3). The total solvent-accessible surface area that was buried upon the interaction was 1,560 Å². The relatively small interface was offset, however, by a high degree of shape complementarity ($S_c = 0.74$, where an S_c value of 1 represents a geometrically perfect fit), which is considerably greater than that typically observed for other NK cell receptor/ligand interactions such as Ly49C-H2-K^b (0.58) (28) or NKG2A/CD94-HLA-E (0.63) (32). The interactions at the TIGIT/nectin-2 interface are primarily

non-polar in nature, with a total of 7 H-bonds and only a single solitary salt bridge (Table 2). The primary points of contact are derived from signature AX₆G lock and TF/YP key interactions derived from the C''C'' and FG loops, respectively. Since TIGIT and nectin-2 possess both a lock and a key, these motifs form complementary interactions that serve to latch the two molecules together (Fig. 2A). Here the prominent aromatic residue of the key (Tyr¹¹³ in TIGIT and Phe¹⁴⁵ in nectin-2) inserts into a concave hydrophobic pocket, making extensive interactions with both main chain and side chain atoms within, and directly after, the AX₆G lock (Ala⁶⁷-Gly⁷⁴ in TIGIT and Ala⁸³-Gly⁹⁰ in nectin-2) (Fig. 3, *A* and *B*). The lock and key interactions, which reside at the periphery of the interface, are further supplemented by additional contacts primarily derived from residues on the face of the more centrally located C-, C'-, and F-sheets (Fig. 3C). Here, the side chains of the second and third positions of a semiconserved VTQ motif (ISL in nectin-2) appear to play a prominent role. In particular, Thr⁵⁵ (in TIGIT) forms a bridge between the C' and C sheets, whereas Gln⁵⁶ extends toward the F-strand forming H-bonds with the hydroxyl of Ser⁶⁶ and the carbonyl of Thr¹⁴⁴ (Fig. 3C).

Structural comparisons

The architecture of the TIGIT/nectin-2 structure is closely related to that previously observed for TIGIT bound to necl-5 D1 (27), as well as that reported for nectin/necl homo- and heterodimers (26) (Fig. 4A). For example, the r.m.s. deviations between TIGIT:nectin-2 D1 and TIGIT:necl-5 D1 is 1.48 Å over all C α atoms. In addition to the overall docking mode, the molecular interactions at the TIGIT/nectin-2 interface, namely those derived from the aromatic key, hydrophobic lock, and (I/V)(S/T)(L/Q) motif, mirror those observed in TIGIT:necl-5 as well as those reported for receptor-receptor (TIGIT:TIGIT) and ligand-ligand (nectin-2:nectin-2) homodimers. Despite this conservation, subtle differences at the interfaces can also profoundly impact binding affinity. For example, whereas nectin-2 forms a tight homodimer ($K_D = 0.4 \mu\text{M}$), TIGIT self-association is very weak ($K_D > 1 \text{ mM}$). Moreover, necl-5 binds to TIGIT with higher affinity than that of nectin-2 (Fig. 1C). To understand the structural basis for the differing affinities of nectin-2 and necl-5 for TIGIT, we overlaid their corresponding structures. Although the vast majority of the structural elements at the interface overlaid closely, we observed a notable difference in the conformation of the C-C' loop (Fig. 4B). In necl-5 this region was closely associated with TIGIT, resulting in a cluster of H-bonding contacts derived from the necl-5 residue Ser⁷⁴ to the carbonyl groups of Pro¹¹⁴ and Asp¹¹⁵ of TIGIT (Fig. 4B). In nectin-2, however, the C-C' loop flexed away from TIGIT such that contacts in this region were limited to only a single nectin-2 residue (Asn⁸¹). Accordingly, the TIGIT/nectin-2 structure provided a plausible explanation for the difference in affinity of nectin-2 and necl-5 for TIGIT.

Energetic basis of the TIGIT/nectin-2 interaction

To further probe the molecular details underpinning TIGIT/nectin-2 specificity we generated a series of nectin-2 mutants and assessed their binding to immobilized TIGIT using SPR (Fig. 5). In tandem we also measured the thermostability of each

Table 2
Contacts between TIGIT and nectin-2

Atomic contacts were determined with CONTACT available within the CCP4i package. Van der Waals (VDW) interactions were defined as non-hydrogen bonded contacts up to a distance of 4 Å. Hydrogen bond and salt bridge interactions were defined as contact distances of less than 3.5 or 4.5 Å, respectively.

TIGIT	Nectin-2	Type
Thr-55 ^{CG2}	Ser-66 ^{CB,O}	VDW
Thr-55 ^{OG1,CG2,OG1}	His-86 ^{NE2,CD2}	VDW
Gln-56 ^{OE1}	Ser-66 ^{OG}	H-Bond
Gln-56 ^{NE2,CB,CD,OE1}	Ser-66 ^{OG,OG,CB}	VDW
Gln-56 ^{NE2}	Ala-143 ^{CB,C}	VDW
Gln-56 ^{OE1}	Thr-144 ^O	H-Bond
Gln-56 ^{NE2,CD,OE1}	Thr-144 ^{N,O,C}	VDW
Gln-56 ^{OE1}	Phe-145 ^{CB}	VDW
Asn-58 ^{ND2}	Ser-149 ^{OG}	H-Bond
Asn-58 ^{ND2}	Ser-149 ^{N,CB}	VDW
Glu-60 ^{OE1}	Ser-149 ^{OG,CB}	VDW
Ile-68 ^{CG2}	Phe-145 ^{CD2}	VDW
Ile-68 ^{CD1}	Pro-146 ^{O,C}	VDW
Ile-68 ^{CD1}	Gly-148 ^{CA,N}	VDW
Asn-70 ^{ND2}	Ser-66 ^{CB}	VDW
Asn-70 ^{CB}	Phe-145 ^{CD2,CE2}	VDW
Asp-72 ^{OD2}	Tyr-64 ^{OH}	VDW
Leu-73 ^{CD1}	Tyr-64 ^{CB,CG,CD2}	VDW
Leu-73 ^{CB,CD1}	Phe-145 ^{CD1,CB1,CB,CG,CZ}	VDW
Gly-74 ^O	Phe-145 ^{CZ,CE2}	VDW
Trp-75 ^O	Phe-145 ^{CZ}	VDW
His-76 ^{CB}	Phe-145 ^{CZ,CE2}	VDW
His-76 ^{CG,CD2,ND1,CE1,NE2}	Pro-146 ^{CB,O}	VDW
His-111 ^{CE1}	Glu-141 ^{OE1}	VDW
His-111 ^{ND1}	Glu-141 ^{OE1}	Salt bridge
His-111 ^{CG,CD2,ND1}	Ala-143 ^{CB}	VDW
His-111 ^{NE2}	Ser-149 ^{OG}	H bond
His-111 ^{CE1}	Ser-149 ^{OG}	VDW
Thr-112 ^{N,O}	Leu-67 ^{CD2}	VDW
Tyr-113 ^{CB,CG,CD1,CE1}	His-86 ^{CD2,CB}	VDW
Tyr-113 ^{CD2,CE2,CZ,OH}	Met-89 ^{CB,CG,S,D.,O}	VDW
Tyr-113 ^{CE1,CZ,OH}	Gly-90 ^{O,C}	VDW
Tyr-113 ^{OH}	Pro-91 ^O	H bond
Tyr-113 ^{CZ,OH}	Pro-91 ^{O,C}	VDW
Tyr-113 ^{CD1,CE1,CZ,OH}	Ser-92 ^{OG,CB,N}	VDW
Pro-114 ^O	Ser-92 ^{OG}	H bond
Pro-114 ^{CA,C,CB}	Ser-92 ^{OG,CB}	VDW
Pro-114 ^O	Pro-94 ^{CB,CG}	VDW
Asp-115 ^O	Asn-81 ^{ND2,CB,CG}	VDW
Asp-115 ^{C,O}	Pro-94 ^{CG,CB}	VDW
Gly-116 ^{CA,C}	Asn-81 ^{CG,ND2,OD1}	VDW
Thr-117 ^{OG1}	Thr-69 ^{CB,CG2,OG1}	VDW
Thr-117 ^{OG1,CB}	Gln-71 ^{NE2}	VDW
Thr-117 ^N	Asn-81 ^{OD1}	H bond
Thr-117 ^{N,CA,CB,O}	Asn-81 ^{CG,OD1,ND2}	VDW
Thr-117 ^{OG1,CG2}	Glu-141 ^{OE1}	VDW

nectin-2 construct to gain insight as to whether the mutations impacted the stability of the molecules (Table 3). As a negative control we included a mutation (E101A) within a surface-exposed loop that was remote from the TIGIT-binding site. As expected, the E101A mutation did not inadvertently impact TIGIT binding ($K_{D(\text{app})} = 4.9 \pm 0.5 \mu\text{M}$) or the stability of nectin-2 (melting temperature (T_m) = 67.2 °C compared with 68.6 °C for wild type). In contrast, mutation of the nectin-2 aromatic key (F145A) completely abolished TIGIT binding, suggesting this residue was absolutely critical for the interaction. However, mutation of residues within the lock whose side chains project toward the key (H86A, M89A) only moderately reduced TIGIT binding ($K_{D(\text{app})} = 21.0 \pm 1.3$ and $8.7 \pm 1.5 \mu\text{M}$, respectively), indicating that interaction of the key with the TIGIT backbone and/or residues outside the lock (e.g. Ser⁹² in nectin-2) may play important roles in the interaction. Next we tested the impact of mutations of the conserved alanine and glycine residues that cap the AX₆G lock. Here, a G90A mutation severely impacted TIGIT binding ($K_{D(\text{app})} = 47.0 \pm 10$

μM), whereas substitution of Ala⁸³ for Val was relatively well tolerated ($K_{D(\text{app})} = 8.8 \pm 1.3 \mu\text{M}$). However, a less conservative A83R substitution resulted in an ~11-fold reduction in TIGIT binding ($K_{D(\text{app})} = 66 \pm 4.0 \mu\text{M}$). Notably, all of the Ala⁸³ and Gly⁹⁰ mutants were considerably less stable ($T_m < 61$ °C) than wild type nectin-2, suggesting they may play a role in maintaining the structural integrity of the lock. We also assessed the relative importance of certain residues at the center of the TIGIT/nectin-2 interface, outside of the canonical lock and key motifs. Here, mutation of L67A within the (I/V)(S/T)(L/Q) reduced TIGIT binding by ~4-fold ($K_{D(\text{app})} = 24.5 \pm 2.1 \mu\text{M}$), whereas mutation of Glu¹⁴¹, which forms the solitary salt bridge at the interface, did not impact binding ($K_{D(\text{app})} = 4.9 \pm 0.4 \mu\text{M}$). Finally we sought to determine whether the differing affinity of nectin-2 and necl-5 for TIGIT was indeed caused by the C-C' loop, as suggested by the TIGIT/nectin-2 structure. To this end we engineered a mutant form of nectin-2 where the C-C' loop was replaced by that of necl-5. This chimeric construct bound to TIGIT with an affinity that was more similar to necl-5 than nectin-2 ($K_{D(\text{app})} = 2.3 \pm 0.2 \mu\text{M}$) indicating that the necl-5 C-C' loop was able to engender nectin-2 with necl-5-like binding capacity. In contrast, mutation of nectin-2 residue Leu⁶⁷ to a Gln (as found in necl-5) did not impact TIGIT binding affinity ($K_{D(\text{app})} = 5.6 \pm 0.6 \mu\text{M}$).

Discussion

The nectin receptors TIGIT, DNAM-1, and CD96 are emerging as key regulators of NK cell function due to their ability to specifically recognize certain nectin and nectin-like adhesion molecules. For example, TIGIT and DNAM-1 bind to nectin-2 and necl-5, whereas TIGIT also recognizes nectin-3 (16, 33, 34). CD96 also shares the necl-5 ligand in common with TIGIT and DNAM-1, but additionally binds to nectin-1 (16, 35). These receptor/ligand interactions not only facilitate adhesion of NK cells to their targets, but also deliver important signals to the NK cell.

Here we have performed a comprehensive structural and biophysical analysis of the TIGIT/nectin-2 interaction. We found that TIGIT bound relatively tightly to the nectin-2 ectodomain, and that this interaction was dependent solely on the most membrane distal nectin-2 Ig domain. The structure of TIGIT bound to nectin-2 D1 revealed a heterotetrameric assembly where two central TIGIT molecules were flanked by two nectin-2 protomers. Each nectin-2 D1 engaged a single TIGIT via an interface that was markedly similar to that previously observed for TIGIT/necl-5 and as well as for nectin-2/nectin-2 and necl-5/necl-5 homotypic interactions (26, 27). This conservation in docking mode between receptor-ligand and ligand/ligand interactions suggests these binding events are mutually exclusive. Indeed, our MALS data confirmed that although nectin-2 normally forms a stable homodimer in solution, only monomeric nectin-2 is capable of TIGIT binding. This finding suggests that TIGIT is likely able to capture nectin-2 on the cell surface, even if nectin-2 is only transiently accessible due to tight homotypic interactions within the plane of the same membrane (in *cis*). Indeed, in our SPR experiments, binding of nectin-2 to immobilized TIGIT was likely in direct competition with nectin-2 self-

Nectin receptor structure

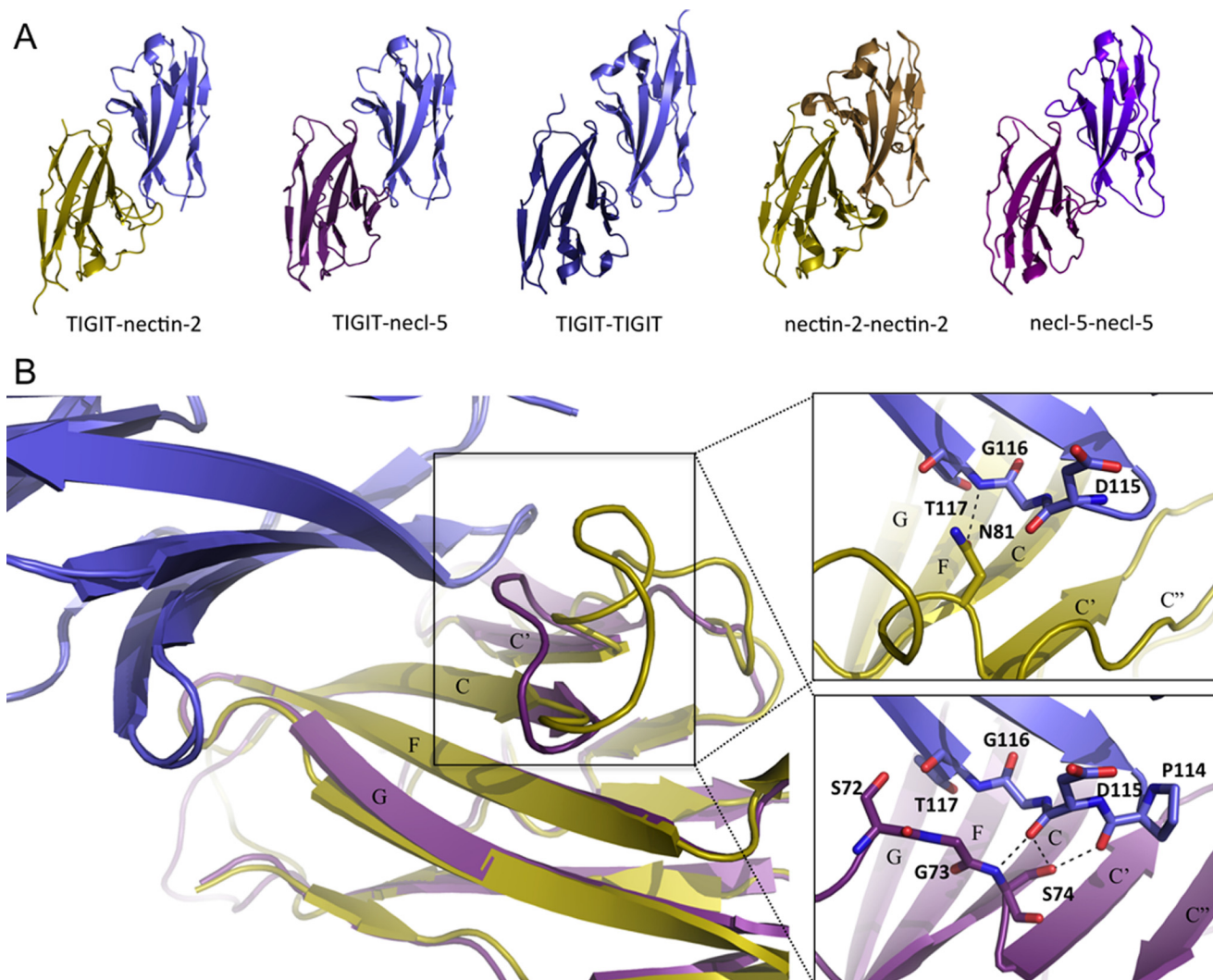


Figure 4. A conserved docking mode in nectin receptors and their ligands. *A*, comparison of the docking modes of nectin receptor-receptor, receptor-ligand, and ligand-ligand complexes. Molecules are colored as follows: TIGIT (slate/blue), nectin-2 (gold/sand), and necl-5 (purple/magenta). PDB accession codes (from left to right) were 5V52, 3UDW, 3RQ3, 4DFH, and 4FQP. *B*, overlay of TIGIT (slate) bound to nectin-2 (gold) and necl-5 (purple) with a view focused on the C-C' loop. The boxed region is magnified on the right, with residues that form direct contacts represented as sticks. Dashed lines indicate hydrogen bonds.

association. For this reason, we report the affinity of the TIGIT/nectin-2 interaction as $K_{D(\text{app})}$.

Intriguingly, the packing of receptor and ligand into a heterotetrameric assembly as observed here was identical to that previously reported for TIGIT/necl-5, despite differences in the space group and unit cell dimensions between the two structures (27). In both cases, two TIGIT molecules associated laterally via their respective A' strands to form a centrally located homodimer that is flanked by the ligand on each side. The recurrence of these structural features might suggest that such an arrangement of receptor and ligand may have physiological relevance outside the bounds of the crystal environment. Indeed, previous studies have suggested that TIGIT self-associates on the cell membrane *in cis* and mutations at the TIGIT-TIGIT homodimer have been reported to inhibit CD155 signaling (27). However, modeling of the TIGIT:nectin-2 hetero-tetramer suggested that this arrangement is unlikely to accommodate a *trans* interaction without a large scale conformational change, although a partially occupied form (TIGIT homodimer bound to a single nectin-2 molecule) could poten-

tially bridge two opposing cell membranes (Fig. 6A). Alternatively, the TIGIT:nectin-2 heterotetramer might also exist *in cis* (Fig. 6B).

To understand the underlying energetic basis for TIGIT/nectin-2 interactions we employed an extensive mutagenesis approach. Here, substitutions of the conserved alanine or glycine residues that cap the AX₆G lock severely impacted TIGIT binding. Notably, mutations here also considerably reduced the thermostability of nectin-2, suggesting that these residues are important for maintaining the structural integrity of the lock. This interpretation is consistent with the associated structural data that indicates these residues point inwards, rather than outwards toward TIGIT. Notwithstanding this, the A83V mutation did not appreciably impact TIGIT binding, suggesting that the AX₆G motif, which represents a defining feature of these receptor and ligand families, can potentially accommodate some variability.

Surprisingly, we observed little to no effect when mutating the residues within the nectin-2 lock, despite these representing the main point of contact for the aromatic key

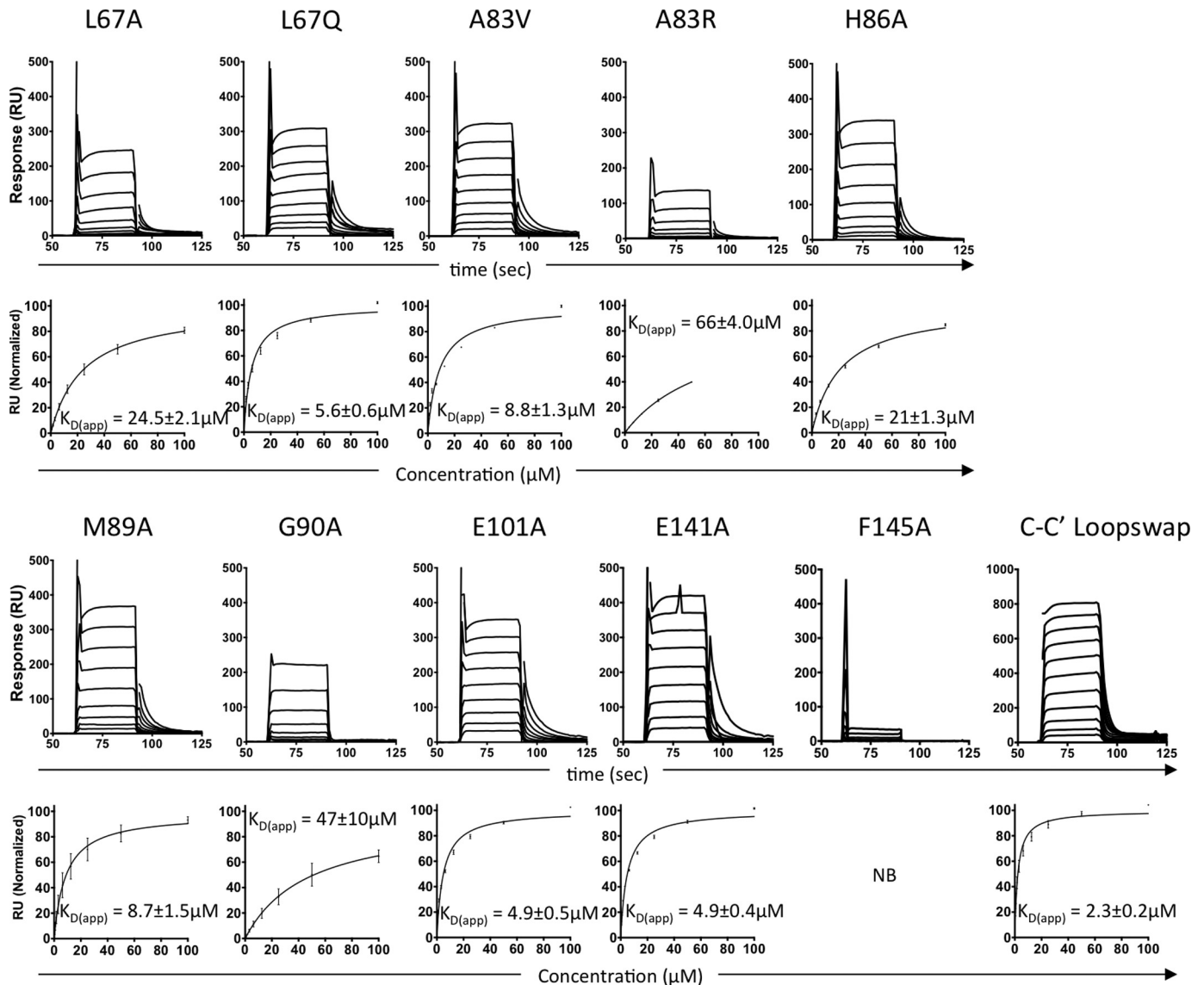


Figure 5. Binding of nectin-2 mutants to TIGIT. SPR sensograms (top rows) and the equilibrium binding curves (bottom rows) of mutants of nectin-2 EC binding to immobilized TIGIT. SPR sensograms are representative of a single experiment. Equilibrium binding curves were derived from 3 (for C-C' loop-swap) or 2 (for all others) independent experiments. $K_D/K_{D(app)}$ and mean \pm S.E. (depicted as error bars) were calculated from the independent experiments. NB indicates no binding.

Table 3
Thermal stability of nectin-2 mutants

Data are representative of two independent thermal melt experiments, each run in duplicate. The mean \pm S.E. was calculated from independent experiments.

Construct	T_m^a ($^{\circ}$ C)	\pm S.E.	Motif
WT	68.61	0.10	
L67A	67.87	0.19	VTQ
L67Q	68.58	0.14	VTQ
A83V	60.68	0.88	Lock
A83R	55.31	0.11	Lock
H86A	61.79	0.51	Lock
M89A	66.68	0.10	Lock
G90A	57.15	0.37	Lock
E101A	67.23	0.43	Control
E141A	66.48	0.09	Salt bridge
F145A	65.49	0.25	Key
Loop swap	66.52	0.18	C-C' loop

^a T_m = melting temperature.

(Phe¹⁴⁵), the mutation of which completely abrogated binding. Although somewhat unexpected, an inspection of the sequence conservation within the AX₆G lock of the nectin

receptors and their ligands (Fig. 1A) indicates that the physicochemical properties of the amino acids located within this region is quite diverse. Thus, rather than their exact nature, the presence of any amino acid side chains that can accommodate the key may be the defining factor that dictates a productive interaction.

Finally, we show that the C-C' loop of the ligand as the major factor governing TIGIT binding hierarchy. Notably, this was the only region that differed appreciably between the first Ig domain of the two TIGIT ligands, nectin-2 and Necl-5. The nectin-2 C-C' loop protruded away from TIGIT, making only limited contacts in contrast to that of necl-5, where it formed an extensive interface. Substitution of the nectin-2 C-C' loop for that of necl-5 improved the affinity of nectin-2 for TIGIT, such that it bound with a similar affinity as necl-5. It will be interesting to determine whether this region similarly impacts binding to the other nectin receptors, CD96 and DNAM-1.

Nectin receptor structure

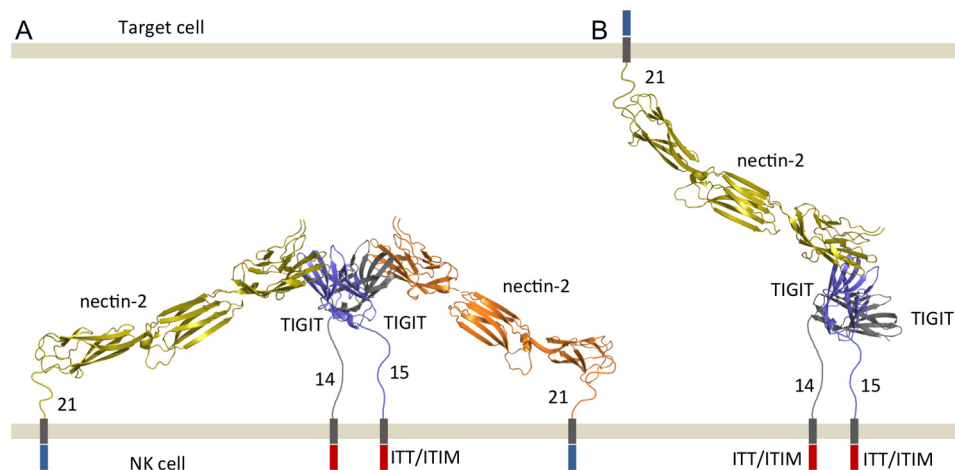


Figure 6. Models of potential TIGIT:nectin-2 arrangements on the cell surface. Models were generated using the nectin-1 ectodomain (orange and gold, PDB accession code 4FMF). A 2 TIGIT:2 nectin-2 heterotetramer is consistent with a *cis* arrangement (A), whereas a 2 TIGIT:1 nectin-2 stoichiometry could be accommodated in *trans* (B). Dark gray boxes represent transmembrane domains, blue/red boxes represent intracellular regions. The length of each membrane proximal stalk is indicated.

Experimental procedures

Protein expression and purification

The gene encoding human TIGIT (encoding amino acid residues 22–128) harboring a mutation of the free cysteine residue (C69S) was cloned into NdeI and NheI restriction sites of the pET30 vector and expressed as inclusion bodies in Tona⁻BL-21 *E. coli* cells as previously described for MHC-I (36). For SPR studies a BirA sequence was inserted at the TIGIT carboxyl terminus. TIGIT was refolded by dilution in a solution containing 4 M urea, 0.4 M L-arginine, 0.1 M EDTA, 0.1 M Tris-HCl, pH 8.0, in 5:1 mM reduced:oxidized glutathione overnight at 4 °C. Refolded TIGIT was dialyzed in 10 mM Tris, pH 8.0, and purified via a combination of anion exchange (using DEAE and HiTrapQ columns) and size exclusion chromatography using a Superdex75 16/60 column (GE Healthcare). For biotinylation, BirA-tagged TIGIT was buffer exchanged into 10 mM Tris, pH 8.0, and biotinylated overnight at 4 °C as previously described (37). The genes encoding the first Ig domain (D1: residues 32–158) and the full-length EC (residues 32–350) of human nectin-2 were cloned into a modified version of the pHLSec vector with C-terminal thrombin-cleavable His₆ tag. Recombinant nectin-2 constructs were expressed via transient transfection in human embryonic kidney 293-S cells as described previously (38). Secreted protein was concentrated and buffer exchanged into 10 mM Tris, pH 8.0, containing 500 mM NaCl and purified via nickel-affinity and size-exclusion chromatography using Superdex 200 16/60 columns (GE Healthcare). All nectin-2 mutants were generated within the context of the entire ectodomain by splice-by-overlap PCR and expressed and purified as described above. The entire ectodomain of human necl-5 (residues 28–334) was cloned into a modified version of the pFastBac vector (Invitrogen) with a C-terminal His₆ tag. Soluble necl-5 was expressed in Hi5 insect cells according to the manufacturers' instructions and purified as described above for nectin-2.

SEC-MALS

50 μ l of TIGIT, nectin-2-EC, or a 1:1 molar ratio of the two proteins at 40 μ M were resolved on a Superdex200 5/150 col-

umn (GE Healthcare) in 10 mM Tris, pH 8.0, 150 mM NaCl at a flow rate of 0.3 ml/min. The system was comprised of DGU-20A₅ degasser, LC-20AD liquid chromatograph, SIL-20AC_{HT} auto sampler, CBM-20A communications bus module, SPD-20A UV-visual detector, and CTO-20AC column oven (Shimadzu) coupled with a DAWN HELIOS-II light scattering detector and Optilab T-rEX refractive index detector (Wyatt). Detector number 12 was substituted for a WyattQELS detector installed at a 90° angle. The system was controlled using LC solutions (Shimadzu) and data collection and analysis were performed ASTRA6 (Wyatt Technology Corp.).

SPR

SPR experiments were performed using a BIAcore 3000 system (GE Healthcare) at 25 °C using a buffer comprising 10 mM Tris, pH 8.0, 150 mM NaCl, and 0.005% surfactant P20. Approximately 500 resonance units of biotinylated TIGIT were immobilized onto streptavidin-coated Sensorchips (GE Healthcare) using standard procedures. All flow cells were quenched with free biotin prior to injection of analytes. Soluble necl-5-EC, nectin-2EC, nectin-2 D1, and mutants thereof were passed over the flow cells in duplicate at a flow rate of 10 μ l/min. The final response was calculated by subtracting the response of an "empty" flow cell (containing biotin blocked streptavidin). Data collection and analysis were performed using BIAevaluation (GE Healthcare) and Prism (GraphPad). Responses from independent experiments were normalized such that the maximal response was defined as 100.

Crystallization and data collection

Purified TIGIT and nectin-2 D1 were mixed at a 1:1 molar ratio at a total protein concentration of 8 mg/ml. Crystals were obtained using the hanging-drop vapor diffusion method from a solution containing 1.3 M lithium sulfate and 0.1 M Tris, pH 7.0. Prior to data collection, crystals were cryoprotected in 0.1 M Tris, pH 7.0, 1.6 M lithium sulfate, and 30% glycerol before being flash-frozen in liquid nitrogen. X-ray diffraction data were recorded on a Quantum-315 CCD detector at the MX2 beamline of the Australian Synchrotron. Data were integrated by

MOSFLM and scaled using SCALA within the CCP4 suite of programs. Details of the data processing statistics are given in Table 1.

Structure determination and refinement

The structure was determined by molecular replacement using Phaser. Monomeric forms of TIGIT and nectin-2 D1, both in unliganded form were used as search models (PDB codes 3UCR and 3R0N, respectively). Because TIGIT and nectin-2 exhibit a large degree of structural similarity, omit maps of the refined structures after deletion of the CC' and DE loops served to validate the identity of the molecules within the crystal lattice. The final structure was solved to reveal a heterotetrameric complex of two TIGIT/nectin-2 dimers and refined to a final R_{fac} of 21.4% and R_{free} 23.0%. Details of the data collection and refinement statistics are in Table 1. The TIGIT/nectin-2 structure has been deposited with the Protein Data Bank (PDB code 5V52).

Thermal melt

The thermal stability of the nectin-2 and mutants thereof was assessed using Rotor Gene Q real-time PCR (Qiagen). Protein samples were added to SYPRO Orange Protein Gel Stain (Sigma) at a final concentration of 0.5 mg/ml and were held at 29 °C for 150 s before the temperature was increased to 90 °C in 1 °C increments. Fluorescence was measured using the yellow channel with the source at 530 nm, detector at 555 nm, and gain of 5. Data acquisition and analysis was done using Rotor Gene Q series software (Qiagen) and Prism (GraphPad), respectively.

Author contributions—F. A. D. designed and performed the experiments, and interpreted the data. B. S. G. assisted with structural determination. J. R. and R. B. conceived and co-led the project. R. B. wrote the manuscript with assistance from F. A. D. and J. R. All authors analyzed the results and approved the final version of the manuscript.

Acknowledgments—We thank Dr. Phillip Pymm for providing purified KIR2DS4 protein as well as the staff at the Monash Macromolecular Crystallization Facility and the Australian Synchrotron for their expert assistance.

References

- Saunders, P. M., Vivian, J. P., O'Connor, G. M., Sullivan, L. C., Pymm, P., Rossjohn, J., and Brooks, A. G. (2015) A bird's eye view of NK cell receptor interactions with their MHC class I ligands. *Immunol. Rev.* **267**, 148–166
- Berry, R., Rossjohn, J., and Brooks, A. G. (2014) The Ly49 natural killer cell receptors: a versatile tool for viral self-discrimination. *Immunol. Cell Biol.* **92**, 214–220
- Brooks, A. G., Posch, P. E., Scorzelli, C. J., Borrego, F., and Coligan, J. E. (1997) NKG2A complexed with CD94 defines a novel inhibitory natural killer cell receptor. *J. Exp. Med.* **185**, 795–800
- Lazetic, S., Chang, C., Houchins, J. P., Lanier, L. L., and Phillips, J. H. (1996) Human natural killer cell receptors involved in MHC class I recognition are disulfide-linked heterodimers of CD94 and NKG2 subunits. *J. Immunol.* **157**, 4741–4745
- Andrews, D. M., Sullivan, L. C., Baschuk, N., Chan, C. J., Berry, R., Cotterell, C. L., Lin, J., Halse, H., Watt, S. V., Poursine-Laurent, J., Wang, C. R., Scalzo, A. A., Yokoyama, W. M., Rossjohn, J., Brooks, A. G., and Smyth, M. J. (2012) Recognition of the nonclassical MHC class I molecule H2-M3 by the receptor Ly49A regulates the licensing and activation of NK cells. *Nat. Immunol.* **13**, 1171–1177
- Borrego, F., Ulbrecht, M., Weiss, E. H., Coligan, J. E., and Brooks, A. G. (1998) Recognition of human histocompatibility leukocyte antigen (HLA)-E complexed with HLA class I signal sequence-derived peptides by CD94/NKG2 confers protection from natural killer cell-mediated lysis. *J. Exp. Med.* **187**, 813–818
- Boyington, J. C., Brooks, A. G., and Sun, P. D. (2001) Structure of killer cell immunoglobulin-like receptors and their recognition of the class I MHC molecules. *Immunol. Rev.* **181**, 66–78
- Sullivan, L. C., Berry, R., Sosnin, N., Widjaja, J. M., Deuss, F. A., Balaji, G. R., LaGruta, N. L., Mirams, M., Trapani, J. A., Rossjohn, J., Brooks, A. G., and Andrews, D. M. (2016) Recognition of the major histocompatibility complex (MHC) class Ib molecule H2-Q10 by the natural killer cell receptor Ly49C. *J. Biol. Chem.* **291**, 18740–18752
- Vivian, J. P., Duncan, R. C., Berry, R., O'Connor, G. M., Reid, H. H., Beddoe, T., Gras, S., Saunders, P. M., Olshina, M. A., Widjaja, J. M., Harpur, C. M., Lin, J., Malveste, S. M., Price, D. A., Lafont, B. A., *et al.* (2011) Killer cell immunoglobulin-like receptor 3DL1-mediated recognition of human leukocyte antigen B. *Nature* **479**, 401–405
- Kärre, K., Ljunggren, H. G., Pirotek, G., and Kiessling, R. (1986) Selective rejection of H-2-deficient lymphoma variants suggests alternative immune defence strategy. *Nature* **319**, 675–678
- Chan, C. J., Martinet, L., Gilfillan, S., Souza-Fonseca-Guimaraes, F., Chow, M. T., Town, L., Ritchie, D. S., Colonna, M., Andrews, D. M., and Smyth, M. J. (2014) The receptors CD96 and CD226 oppose each other in the regulation of natural killer cell functions. *Nat. Immunol.* **15**, 431–438
- Gilfillan, S., Chan, C. J., Cella, M., Haynes, N. M., Rapaport, A. S., Boles, K. S., Andrews, D. M., Smyth, M. J., and Colonna, M. (2008) DNAM-1 promotes activation of cytotoxic lymphocytes by nonprofessional antigen-presenting cells and tumors. *J. Exp. Med.* **205**, 2965–2973
- Martinet, L., and Smyth, M. J. (2015) Balancing natural killer cell activation through paired receptors. *Nat. Rev. Immunol.* **15**, 243–254
- Stanietsky, N., Simic, H., Arapovic, J., Toporik, A., Levy, O., Novik, A., Levine, Z., Beiman, M., Dassa, L., Achdout, H., Stern-Ginossar, N., Tsukerman, P., Jonjic, S., and Mandelboim, O. (2009) The interaction of TIGIT with PVR and PVRL2 inhibits human NK cell cytotoxicity. *Proc. Natl. Acad. Sci. U.S.A.* **106**, 17858–17863
- Stanietsky, N., Rovis, T. L., Glasner, A., Seidel, E., Tsukerman, P., Yamin, R., Enk, J., Jonjic, S., and Mandelboim, O. (2013) Mouse TIGIT inhibits NK-cell cytotoxicity upon interaction with PVR. *Eur. J. Immunol.* **43**, 2138–2150
- Yu, X., Harden, K., Gonzalez, L. C., Francesco, M., Chiang, E., Irving, B., Tom, I., Ivelja, S., Refino, C. J., Clark, H., Eaton, D., and Grogan, J. L. (2009) The surface protein TIGIT suppresses T cell activation by promoting the generation of mature immunoregulatory dendritic cells. *Nat. Immunol.* **10**, 48–57
- Liu, S., Zhang, H., Li, M., Hu, D., Li, C., Ge, B., Jin, B., and Fan, Z. (2013) Recruitment of Grb2 and SHIP1 by the ITT-like motif of TIGIT suppresses granule polarization and cytotoxicity of NK cells. *Cell Death Differ.* **20**, 456–464
- Hsu, J. L., van den Boomen, D. J., Tomasec, P., Weekes, M. P., Antrobus, R., Stanton, R. J., Ruckova, E., Sugrue, D., Wilkie, G. S., Davison, A. J., Wilkinson, G. W., and Lehner, P. J. (2015) Plasma membrane profiling defines an expanded class of cell surface proteins selectively targeted for degradation by HCMV US2 in cooperation with UL141. *PLoS Pathog.* **11**, e1004811
- Matusali, G., Potestà, M., Santoni, A., Cerboni, C., and Doria, M. (2012) The human immunodeficiency virus type 1 Nef and Vpu proteins downregulate the natural killer cell-activating ligand PVR. *J. Virol.* **86**, 4496–4504
- Tomasec, P., Wang, E. C., Davison, A. J., Vojtesek, B., Armstrong, M., Griffin, C., McSharry, B. P., Morris, R. J., Llewellyn-Lacey, S., Rickards, C., Nomoto, A., Sinzger, C., and Wilkinson, G. W. (2005) Downregulation of natural killer cell-activating ligand CD155 by human cytomegalovirus UL141. *Nat. Immunol.* **6**, 181–188
- Gromeier, M., Lachmann, S., Rosenfeld, M. R., Gutin, P. H., and Wimmer, E. (2000) Intergeneric poliovirus recombinants for the treatment of malignant glioma. *Proc. Natl. Acad. Sci. U.S.A.* **97**, 6803–6808

Nectin receptor structure

22. Masson, D., Jarry, A., Baurly, B., Blanchardie, P., Laboisse, C., Lustenberger, P., and Denis, M. G. (2001) Overexpression of the *CD155* gene in human colorectal carcinoma. *Gut* **49**, 236–240
23. Oshima, T., Sato, S., Kato, J., Ito, Y., Watanabe, T., Tsuji, I., Hori, A., Kurokawa, T., and Kokubo, T. (2013) Nectin-2 is a potential target for antibody therapy of breast and ovarian cancers. *Mol. Cancer* **12**, 60
24. Sloan, K. E., Eustace, B. K., Stewart, J. K., Zehetmeier, C., Torella, C., Simeone, M., Roy, J. E., Unger, C., Louis, D. N., Ilag, L. L., and Jay, D. G. (2004) CD155/PVR plays a key role in cell motility during tumor cell invasion and migration. *BMC Cancer* **4**, 73
25. Long, E. O., Burshtyn, D. N., Clark, W. P., Peruzzi, M., Rajagopalan, S., Rojo, S., Wagtmann, N., and Winter, C. C. (1997) Killer cell inhibitory receptors: diversity, specificity, and function. *Immunol. Rev.* **155**, 135–144
26. Harrison, O. J., Vendome, J., Brasch, J., Jin, X., Hong, S., Katsamba, P. S., Ahlsen, G., Troyanovsky, R. B., Troyanovsky, S. M., Honig, B., and Shapiro, L. (2012) Nectin ectodomain structures reveal a canonical adhesive interface. *Nat. Struct. Mol. Biol.* **19**, 906–915
27. Stengel, K. F., Harden-Bowles, K., Yu, X., Rouge, L., Yin, J., Comps-Agrar, L., Wiesmann, C., Bazan, J. F., Eaton, D. L., and Grogan, J. L. (2012) Structure of TIGIT immunoreceptor bound to poliovirus receptor reveals a cell-cell adhesion and signaling mechanism that requires cis-trans receptor clustering. *Proc. Natl. Acad. Sci. U.S.A.* **109**, 5399–5404
28. Dam, J., Guan, R., Natarajan, K., Dimasi, N., Chlewicki, L. K., Kranz, D. M., Schuck, P., Margulies, D. H., and Mariuzza, R. A. (2003) Variable MHC class I engagement by Ly49 natural killer cell receptors demonstrated by the crystal structure of Ly49C bound to H-2K(b). *Nat. Immunol.* **4**, 1213–1222
29. Aguilar, O. A., Berry, R., Rahim, M. M., Reichel, J. J., Popović, B., Tanaka, M., Fu, Z., Balaji, G. R., Lau, T. N., Tu, M. M., Kirkham, C. L., Mahmoud, A. B., Mesci, A., Krmpotić, A., Allan, D. S., *et al.* (2017) A viral immunoevasin controls innate immunity by targeting the prototypical natural killer cell receptor family. *Cell* **169**, 58–71 e14
30. Bork, P., Holm, L., and Sander, C. (1994) The immunoglobulin fold. Structural classification, sequence patterns and common core. *J. Mol. Biol.* **242**, 309–320
31. Liu, J., Qian, X., Chen, Z., Xu, X., Gao, F., Zhang, S., Zhang, R., Qi, J., Gao, G. F., and Yan, J. (2012) Crystal structure of cell adhesion molecule nectin-2/CD112 and its binding to immune receptor DNAM-1/CD226. *J. Immunol.* **188**, 5511–5520
32. Petrie, E. J., Clements, C. S., Lin, J., Sullivan, L. C., Johnson, D., Huyton, T., Heroux, A., Hoare, H. L., Beddoe, T., Reid, H. H., Wilce, M. C., Brooks, A. G., and Rossjohn, J. (2008) CD94-NKG2A recognition of human leukocyte antigen (HLA)-E bound to an HLA class I leader sequence. *J. Exp. Med.* **205**, 725–735
33. Bottino, C., Castriconi, R., Pende, D., Rivera, P., Nanni, M., Carnemolla, B., Cantoni, C., Grassi, J., Marcenaro, S., Reymond, N., Vitale, M., Moretta, L., Lopez, M., and Moretta, A. (2003) Identification of PVR (CD155) and Nectin-2 (CD112) as cell surface ligands for the human DNAM-1 (CD226) activating molecule. *J. Exp. Med.* **198**, 557–567
34. Tahara-Hanaoka, S., Shibuya, K., Onoda, Y., Zhang, H., Yamazaki, S., Miyamoto, A., Honda, S., Lanier, L. L., and Shibuya, A. (2004) Functional characterization of DNAM-1 (CD226) interaction with its ligands PVR (CD155) and nectin-2 (PRR-2/CD112). *Int. Immunol.* **16**, 533–538
35. Seth, S., Maier, M. K., Qiu, Q., Ravens, I., Kremmer, E., Förster, R., and Bernhardt, G. (2007) The murine pan T cell marker CD96 is an adhesion receptor for CD155 and nectin-1. *Biochem. Biophys. Res. Commun.* **364**, 959–965
36. Berry, R., Vivian, J. P., Deuss, F. A., Balaji, G. R., Saunders, P. M., Lin, J., Littler, D. R., Brooks, A. G., and Rossjohn, J. (2014) The structure of the cytomegalovirus-encoded m04 glycoprotein, a prototypical member of the m02 family of immunoevasins. *J. Biol. Chem.* **289**, 23753–23763
37. Berry, R., Ng, N., Saunders, P. M., Vivian, J. P., Lin, J., Deuss, F. A., Corbett, A. J., Forbes, C. A., Widjaja, J. M., Sullivan, L. C., McAlister, A. D., Perugini, M. A., Call, M. J., Scalzo, A. A., Degli-Esposti, M. A., *et al.* (2013) Targeting of a natural killer cell receptor family by a viral immunoevasin. *Nat. Immunol.* **14**, 699–705
38. Aricescu, A. R., Lu, W., and Jones, E. Y. (2006) A time- and cost-efficient system for high-level protein production in mammalian cells. *Acta Crystallogr. D Biol. Crystallogr.* **62**, 1243–1250